The hydrogen isotopic composition and water content of southern Pacific MORB: A reassessment of the D/H ratio of the depleted mantle reservoir

Matthieu Clog, Cyril Aubaud, Pierre Cartigny, Laure Dosso

Earth and Planetary Science Letters
November 2013, Volume 381, Pages 156–165
http://dx.doi.org/10.1016/j.epsl.2013.08.043

The hydrogen isotopic composition and water content of southern Pacific MORB: A reassessment of the D/H ratio of the depleted mantle reservoir

Matthieu Clog[a, 1, *], Cyril Aubaud[a], Pierre Cartigny[a], Laure Dosso[b]

[a] Laboratoire de Géochimie des Isotopes Stables, Institut de physique du Globe, Université Paris 7 Denis Diderot, CNRS (UMR 7154), PRES Sorbonne Paris Cité, 1, rue Jussieu, 75005 Paris, France
[b] CNRS-UMR 6538, Domaines Océaniques, IFREMER, B.P. 70, 29280 Plouzané, France

[1] Present address : GPS Division, California Institute of Technology, Pasadena, CA, USA.

*: Corresponding author : Matthieu Clog, email address : clog@caltech.edu

Abstract:

In this paper, we re-investigate the isotopic composition of hydrogen in MORB and the possible effects of contamination on δD and water content. A suite of 40 N-MORB from the Pacific–Antarctic ridge, far from any hotspot, was analyzed for chlorine content by electron microprobe and for water content and δD with silica tubes. Cl concentrations (from 29 to 2400 ppm) indicate widespread contamination, more intense with faster spreading rates, while water contents (from 840 to 7800 ppm) are mainly controlled by igneous processes. δD values range from −76 to −48‰, with an average value of −61‰. The lack of correlation between Cl content and either H_2O/Ce or δD indicate that contamination has a negligible effect on δD for our samples, which is therefore characteristic of the mantle below the Pacific–Antarctic ridge. We suggest that the 20‰ lower δD value reported for the North Pacific and North Atlantic is highly unlikely from geodynamical arguments. We propose that the convecting mantle is characterized by a δD of −60±5‰, as supported by the most recent data from North Atlantic N-MORB.

Highlights

► A suite of 40 MORB was analyzed for δD, water and Cl content. ► Degassing and contamination have negligible effect on D/H. ► Average δD is ∼−60‰, 15‰ higher than earlier studies. ► High regional D are unlikely, analytical artifacts may be responsible. ► We propose an updated value for mantle D/H.

Keywords: hydrogen isotopes ; mantle geochemistry ; mantle water

1. Introduction

Based on the pioneer work of Kyser and O'Neil (1984), the isotopic composition of hydrogen in the convective mantle is commonly assumed to be characterized by a δD of -80$\pm$10‰ (compared to SMOW). The D/H variations were attributed to secondary processes, especially contamination by seawater and seawater-derived fluids, both with higher δD than the mantle. Hence, in any given area, the value most likely to characterize mantle hydrogen would be the lowest observed, typically -80‰. Several studies (Poreda et al., 1986; Kingsley et al., 2002; Pineau et al., 2004) have however since shown co variations between δD-values (ranging from -80 to -40‰) and tracers of mantle source heterogeneities (either ratios of rare-earth elements or Pb isotopes), demonstrating that source heterogeneity rather than contamination is the main factor controlling the variations of δD and H_2O in MORB, OIB and seamount chain basalts. This is also consistent with studies of water to light rare earth element ratios of similar incompatibilities (Michael, 1995; Kent et al., 1999b; Danyushevsky et al., 2000; Le Roux et al., 2006), which showed that MORB H_2O/Ce (or /La) are regionally homogeneous and characteristic of the local MORB mantle source. How δD-values may vary remain however typically unaddressed (except for Kingsley et al. (2002)). Moreover, a recent study has shown that extracting water by induction heating of basaltic glasses in a Pt-crucible (which was the prefered method in the 80's, Kyser and O'Neil (1984)) can lower the measured δD by more than 10‰ (Clog et al., 2012). It further illustrates the need to re-evaluate the hydrogen isotopic composition of the mantle and its variability.

In the present study we reinvestigate the current consensus that the δD-

value of the MORB mantle is equal to -80‰ and propose that a value of ≈-60‰ is more appropriate.

2. Samples locality background and analytical techniques

The Pacific-Antarctic ridge is ideal to re-investigate the D/H isotope composition of the depleted upper mantle. Two large supersegments (from 65 to 56°S and from 52 to 41°S, sampled respectively by the French missions PACANTARCTIC 1 (1996) and 2 (2005)) present MORB compositions characterizing a rather homogeneous mantle devoid of hotspot influence (see Vlastélic et al. (2000) for the southern one ; Moreira et al. (2008) and Hamelin et al. (2010) for the northern one). They are separated by a region with several fracture zones which record interactions with the Louisville hotspot, as illustrated by the greater variability of MORB compositions in radiogenic isotope ratios (Castillo et al., 1998; Géli et al., 1998; Vlastélic et al., 1998). Spectral analysis of the variations in isotopic compositions of Pb, Sr and Nd along the Pacific-Antarctic and East-Pacific ridges showed that the composition of MORB from those supersegments reflects subtle variations within the range of N-MORB compositions, consistent with a gradual greater contribution of the HIMU component northwards (Hamelin et al., 2011).

Except for helium analyses (Moreira et al., 2008; Hamelin et al., 2011), which show homogeneous isotopic composition typical of the depleted mantle (R/R_a=7.29±0.19), there has been no study of volatile elements in this region. Moreira et al. (2008) also noted limited variations and in particular that the northern supersegment is the most homogeneous ridge portion studied with respect to He isotopic compositions.

The variations in structure and spreading rate in this area are also of importance. The spreading rate increases northwards, from 54 mm/yr at 70°S to 111 mm/yr at 40°S (DeMets et al., 1990) and is associated with a change in the structure of the ridge in the southern supersegment, from a central valley typical of slow-spreading ridges to a central dome typical of faster ridges. As noted by Vlastélic et al. (2000), the morphology appears to be primarily controlled by the spreading rate, rather than by the potential mantle temperature. On the whole northern supersegment, the structure is typical of a fast-spreading ridge (Klingelhoefer et al., 2006; Hamelin et al., 2010). Faster ridges have typically more important and widespread hydrothermal circulation, leading to a more pronounced chlorine contamination (Michael and Cornell, 1998; Bonifacie et al., 2008). Therefore, for water studies, the structure of the ridge could also be of importance, particularly in assessing the effect of contamination of seawater derived-fluids on δD-values.

2.1. Sample suite

All samples in this study are glassy rims of pillow lavas dredged at the axis of the ridge, at depths between 1500 and 2800 meters below sea level, except PAC1CV07 which was dredged on an off-axis seamount (figure 1).

Forty basalts were analyzed for water and chlorine contents, and for δD. All the samples are N-MORB (La/Sm_N <1, where $_N$ marks normalization to the primitive mantle, McDonough and Sun (1995)), with a slightly higher alkali content for samples collected near the Menard Transform Fault Fracture (samples PAC2 DR7 and PAC2 DR20) due to greater extents of crystal fractionation. Most samples were previously analyzed for their compositions in major (n = 37), trace (n = 35) and radiogenic (Sr, Nd, Pb) elements iso-

topic compositions (n = 37) and some (n = 16) for helium concentrations and isotopic compositions (tables 1 and 2, Vlastélic et al. (1999, 2000); Moreira et al. (2008); Hamelin et al. (2010, 2011)). We report new cerium data measured by NAA (Neutron Activation Analysis) for the samples of the southern supersegment, with the same technique as used for La and Sm by (Vlastélic et al., 2000). Tables 3 and 4 report the δD, H_2O, Cl and Ce concentrations, along with geographic coordinates and depth of collection.

2.2. Water content and δD measurements

The technique used in this study has been described in Clog et al. (2012) and is summarized here. It is based on the original method described by Vennemann and O'Neil (1993). Glass samples were crushed to shards of 100 to 250 μm, washed in distilled water, ultrasonically cleaned and dried. Most of the plagioclase, olivine and altered grains were discarded using a Frantz magnetic sorting apparatus. Remaining minerals and altered chips were removed by careful handpicking under a binocular, to select only fresh glass shards.

The mass of sample typically used was 350 mg for each analysis. The sample was introduced into a pre-cleaned sealed quartz tube (2 hours at 1150°C) connected to a vacuum line and heated to 250°C for half an hour to eliminate any adsorbed water. Then the samples were heated to 950°C for 45 minutes under a pressure of 400 Pa of pure O_2 obtained by thermal decomposition of CuO. The released CO_2 and H_2O (and other condensable gases such as SO_2) are held in a cold trap at -196°C (liquid nitrogen) and separated by setting the temperature at -140°C to keep only H_2O, while incondensable gases and CO_2 are pumped out of the line. Water is then reduced on hot uranium fur-

nace held at 800°C to obtain H_2 (Bigeleisen et al., 1952). The amount of gas is measured by manometry and it is then concentrated into a sampling tube with a Toepler pump. The gas is analyzed with a dual-inlet mass spectrometer (Delta Plus XP). The typical reproducibility on the measurements was $\pm$5% for water content and $\pm$3‰ for δD (both 2σ, as established from the 10 analysis of the PAC2DR20-1-1 sample). Procedural blanks amount to $\approx$0.4 μmol. Re-heating a sample that had previously been heated to 900°C for half an hour produced amounts of water equal to the value of our experimental blanks, demonstrating that we reached quantitative water recovery.

The uranium furnace was calibrated with three standard waters : ROSS (δD=-114.9‰), EPB-5 (δD=-44.4‰) and ORSMOW (δD=+2.4‰). These in-house standards were obtained from the LSCE (Laboratoire des Sciences du Climat et l'Environnement, Saclay, France) where they are regularly calibrated against IAEA standards (VSLAP, δD=-428‰ and VSMOW, δD=0‰). During the course of this study, we checked the accuracy of our analytical protocol by regularly measuring the δD-value of the standard NBS-30. We obtain an average value of -63.4$\pm$2‰ (2σ, n=6), in agreement, within analytical uncertainties, with the recommended value of -65.7$\pm$0.6‰ (2σ).

All samples were at least duplicated, reported values representing their averages, and all were within $\pm$3‰.

2.3. Chlorine content measurements

Fresh glass shards were mounted in epoxy and polished for analysis. Chlorine concentrations were determined using electron microprobe with a CAMECA SX50 at the CAMPARIS analytical facility in Paris, France, using well-established techniques (e.g. Jambon et al., 1995). Analyses were made

using a 20 μm diameter, 500 nA electron beam intensity, at 30 kV acceleration voltage and with a counting time of 60 s for chlorine and for backgrounds. All four spectrometers were used simultaneously. Calibration was determined using a scapolite standard (Cl content 4.04 wt%). Ten points were measured for each sample along a transect, avoiding visible cracks or imperfection in the polished surface. The detection limit is 13 ppm, as determined on an olivine standard and the reproducibility in chlorine concentration range from 5 to 10 ppm (1 σ).

3. Results

3.1. Water concentrations

Water concentrations range from 840 to 7800 ppm (n = 40), which is within the typical range for MORB (2300^{+3500}_{-1600} ppm, PetDB database (Lehnert et al., 2000) and Kyser and O'Neil (1984); Poreda et al. (1986); Jambon and Zimmermann (1990); Pineau and Javoy (1994); Michael (1995); Dixon et al. (2002); Pineau et al. (2004); Le Roux et al. (2006)). High water samples are rare, with only four having more than 4000 ppm H_2O (tables 3 and 4, figure 2b). H_2O/Ce ratios range from 112 to 254 (figure 3a, 186±30 on the southern supersegment and 173±15 on the northern supersegment), within the range observed in MORB (from 100 to 350, Michael (1995)). The typical range for Pacific MORB is 180±30 (Michael, 1995; Le Roux et al., 2006), and only samples south of 63°S present H_2O/Ce ratios outside this range. No systematic variation of water content or H_2O/Ce with latitude was found (figure 2).

3.2. Hydrogen isotopic compositions

δD range from -76 to -48‰ (tables 3 and 4, figure 2a), within the range of previously studied MORB (from -92 to -44‰ (Kyser and O'Neil, 1984; Poreda et al., 1986; Chaussidon et al., 1991; Pineau and Javoy, 1994; Kingsley et al., 2002; Pineau et al., 2004; Hauri et al., 2006b; Cartigny et al., 2008)). The δD values show no significant correlation to either water contents or water to cerium ratios. It is however worth noting that more than >90% of the N-MORB from the North Pacific and Atlantic previously published have δD between -85 and -65 ‰ (Kyser and O'Neil, 1984; Pineau et al., 2004; Hauri et al., 2006b; Cartigny et al., 2008). The values measured here are thus more comparable to previously analyzed E-MORB from other oceanic basins (Poreda et al., 1986; Kingsley et al., 2002), though N-MORB from the East Pacific Rise near 22°N and the west rift of the Easter microplate have δD close to -65‰ (Kingsley et al., 2002). There is also no correlation with Sr, Nd, Hf Pb or He isotope data on theses samples (figure 3b) or with the La/Sm ratio.

3.3. Chlorine concentrations

Cl concentrations vary from 23 to 2000 ppm (figure 3c), within the MORB range (from 10 (below the detection level) to more than 4000 ppm (Jambon et al., 1995; Michael and Cornell, 1998; Soule et al., 2006), 90% of measured MORB falling below 800 ppm (PetDB database)). On average, samples from the northern supersegment, where the spreading rate is higher, have higher Cl/K than samples from the southern supersegment (modes $0.32^{+0.58}_{-0.21}$ vs $0.16^{+0.22}_{-0.09}$, figure 3d). Potassium and chlorine having similar bulk partition

coefficient during partial melting and crystal fractionation (Michael and Cornell, 1998), the variations are thus too large to depend only upon variations in igneous processes, but reflect contamination or assimilation, as discussed in the next section.

4. Discussion

4.1. Degassing

Contrary to CO_2 which can degas at high pressure, water is much more soluble in silicate melts and typically remains under-saturated in typical MORB settings (e.g., Dixon and Stolper, 1995; Jendrzejewski et al., 1996). Kyser and O'Neil (1984) suggested that loss of hydrogen could occur either as degassing of H_2 or CH_4. Subsequent studies have actually shown that MORB are more oxydized than was originally thought (Bézos and Humler, 2005; Kelley and Cottrell, 2009), and therefore, H_2/CH_4 degassing is not significant. Furthermore all samples present very low vesicularity (<1%), are under-saturated with respect to water (figure 4), and can be calculated to be in equilibrium with a gas phase containing less than 5% of water for all but 4 of the samples. The sample PAC1DR10-1 is in equilibrium with a vapor phase containing more than 20% of water, and is thus the most likely to have experienced some degassing. However, its δD is indistinguishable from the δD of the sample PAC1DR10-2 which comes from the same dredge and argues against any significant degassing-induced change in δD values. The homogeneity of the H_2O/Ce ratios observed along the supersegments is also a compelling argument against degassing. Degassing of water thus appears negligible for all of our samples.

4.2. Effects of contamination on volatile contents

It should be first noted that previous studies established that variations in major and trace elements in this sample suite are mostly due to crystal fractionation (Vlastélic et al., 2000; Hamelin et al., 2010). This is also illustrated by the evolution of La and Ce content with MgO wt% (figure 5a and b). In this section we investigate to what extent are non-igneous processes responsible for variations in water and chlorine content.

Ratios of Cl and H_2O to elements of similar incompatibilities (typically K, La or Ce) can be used to quantify the degree of interaction with brines or hydrated rocks during ascent (e.g., Michael, 1995; Michael and Cornell, 1998). This is because contamination of lavas by seawater-derived fluids results in an increase in chlorine content, while water content appears comparatively less (or not) affected (Michael and Cornell, 1998; Kent et al., 1999a,b; Dixon and Clague, 2001; Soule et al., 2006).

Constraining the interaction with brines or hydrated rock on the basis of the δD alone is difficult, as the isotopic composition of the brines deep in the crust is unconstrained, while hydrated rocks can have δD similar to those measured in our samples (e.g., Agrinier et al., 1995). It is worth noting that experiments led to the suggestion that high-Cl brines should be depleted in D, with $\Delta D_{vapor-brine}$ fractionation between 2 and 8‰ according to Berndt et al. (1996), but the same study also highlighted the difficulty in trying to relate the measured fractionation and the δD of outwards fluxes at hydrothermal vents due to uncertainties in mixing processes, temperature of the reaction, closed versus open system consideration and concurrent processes of interaction with the crustal rocks. In summary, from available studies, the D/H

ratio of brines is still difficult to anticipate. Yet, it should also be noted that contamination by either brines or hydrothermally altered rocks cannot buffer the δD of our samples as they are all under-saturated with respect to water.

In the following discussion, we therefore focus on the the H_2O/Ce and Cl/K ratios.

4.2.1. H_2O/Ce ratios

Water content increases smoothly with decreasing MgO wt% (figure 5c), suggesting that water content is primarily controlled by igneous processes rather than contamination. We also observed that the H_2O/Ce ratios are rather homogeneous on our sample suite. The average H_2O/Ce ratio is $\approx$185$\pm$30 on the southern supersegment and $\approx$175$\pm$15 on the northern one, which is, within this small range, the opposite of what would be expected from the relationship between ridge structure and degree of assimilation (Michael and Cornell, 1998). All this evidence argues against substantial hydrogen contamination by either seawater-derived fluids or hydrated rocks during ascent (see also figure 6).

4.2.2. Cl/K ratios

Contrary to water, the chlorine content variations cannot be explained solely by crystal fractionation (figure 5d). We observe that the majority of samples have incurred a greater extent of crystal fractionation (MgO<7.5 wt.%) have Cl content much higher than the crystal fractionation trend, which contrasts with samples where MgO>8.0 wt.%. Cl/K ratios are also higher in the northern supersegment (modes $0.32^{+0.58}_{-0.21}$ in the northern supersegment and $0.16^{+0.22}_{-0.09}$ in the southern supersegment, figure 3d), which

points to more intense contamination with an increasing spreading rate, as has been proposed by Michael and Cornell (1998) and Bonifacie et al. (2008). It should be noted that this difference is however mostly driven by a couple of extremely Cl-enriched samples (PAC2 DR34-1 and PAC2 DR28-2).

A recent study (Kendrick et al., 2012), based on a global compilation of Cl and K concentrations, has proposed that the average Cl/K of uncontaminated MORB is close to 0.08. When comparing to modes of 0.16 and 0.32 on respectively the southern and northern supersegments, this would indicate that our samples are extensively contaminated with respect to Cl. Conversely, the lowest Cl/K measured on our samples are, for both segments, $\approx$0.03, illustrating the non-uniformity of the contamination. This would imply, for chlorine budget, that the details of the ascent and eruption scenarii are at least of equal importance to the spreading rate. Lowest Cl/K were observed in both cases where the magmatic activity is less vigorous : a near-axis seamount in the south and a sample from the S2 segment, whose structure is described as poorly defined (Hamelin et al., 2010) due to interaction with the Menard Fracture Zone in the north. Assuming that the smallest Cl/K measured correspond to uncontaminated samples, we conclude that more than 80% of Cl comes from contamination in our sample suites (versus more than 50% of Cl from contamination if we use the average value of Kendrick et al. (2012)).

The contrast between the behavior of water and chlorine suggests that contamination in our sample suite is not due to assimilation of hydrated wall-rock or contribution from seawater or diluted brines, but due to either very concentrated brines or pure halite left in the crust by hydrothermal

circulation (figure 6). It should also be noted that samples with low Cl content (<100 ppm, 12 samples) or low Cl/K (<1.6, 12 samples) present a range of δD from -76 to -51‰, and an average δD of -63‰. Those values are close to those observed for the complete sample suite (δD from -75 to -48‰ and $\delta\bar{\text{D}} \approx$-61‰. This is consistent with a very minor effect of contamination on the D/H ratio of our samples.

4.3. Incompatibility of water relative to La and Ce

Although it is well described that the bulk partition coefficient of water during mantle partial melting is close to Ce and La (Michael, 1995), the rare-earth element whom behavior is closest to water actually depends on the degree of enrichment of the source in incompatible elements (Danyushevsky et al., 2000). In the extreme case of Macquarie Island, where the primitive, weakly fractionated basalts have $(\text{La/Sm})_\text{N} > 2$, it was recently proposed that Pr was the element whose behavior was the most similar to water (Kamenetsky and Eggins, 2012), emphasizing the need to carefully choose the element for normalization.

For our sample suite, the incompatibility of water is more closer to that of Ce rather than of La, as illustrated on figure 7. The regression line defined by our samples in H_2O/Ce-Ce space is actually flatter (slope of -0.6±0.7, origin 190±12) than the one in H_2O/La-La space (slope -13±9, origin 624±54). This justifies the normalization to Ce rather than La chosen in the previous section as well as in the rest of this article.

Considering the range of $(\text{La/Sm})_\text{N}$ observed here (between 0.45 and 0.95), our results contrasts with those of Danyushevsky et al. (2000) which suggested that La should be more appropriate. It should be noted that there

is no requirement for disagreement. Partition coefficient for individual minerals (olivine, garnet, pyroxene) are not similar between water and La/Ce (Aubaud et al., 2004; Hauri et al., 2006a; Kohn, 2006; Grant et al., 2007). Therefore source mineralogy affect the bulk partition coefficient for H_2O, La or Ce, and as a matter of consequence, the preference for Ce over La in this sample suite.

4.4. Crystal fractionation and partial melting effects

In the southernmost area, the H_2O/Ce ratio is more variable (standard deviation of 50 south of the Saint-Exupery fracture zone versus standard deviation of 15 for the rest of the sample set, see also figure 3). This could mean that the source region is heterogeneous at the scale of sampling (≈100 km between two samples). We also observe that the average MgO% is higher (≈8.1 versus ≈6.9). This is indicative of more primitive melts, and an alternative model to heterogeneities in the source is that we observe un-mixed melting products of an heterogeneous source, as proposed by Langmuir and Bender (1984), and that northwards, those melts are pooled in magma chambers where they differenciate before eruption.

We calculated the water content of the source by correcting to 8% of MgO (Weaver and Langmuir, 1990; Kelley et al., 2006) and using a simple batch melting model, assuming a constant Na content of the source. The results are illustrated in figure 8, whose caption contains the details of the calculation.

For most (>80%) of the samples, the calculated water content is in the range 150-250 ppm. The obvious limitations of this method are the assumed homogeneity of Na content and the variations of solidus temperature with water content. A posteriori, the influence of the latter is negligible consid-

ering the limited range of calculated H_2O_{source}. The variations observed in water content are thus consistent with a source containing 200±50 ppm of water with an extent of melting between 8 and 10%, followed by various extents of crystal fractionation.

Despite the relative homogeneity of our sample suite, we discuss in the next section the consequence of melting a heterogeneous mantle source in terms of δD-variability.

4.5. Hydrogen heterogeneities in the source

As water behaves as a very incompatible element during igneous processes ($D_{peridotite-melt}$ ≈0.012 Aubaud et al., 2004; Kohn, 2006; Grant et al., 2007), hydrogen isotopes are not significantly fractionated during melting at ridges (where the extent of melting is typically higher than 5%, Asimow and Langmuir (2003)) and crystal fractionation, even though the isotopic fractionation factor of H between liquid and silicate minerals is higher than 10‰ at magmatic temperatures (Dobson et al., 1989; Bell and Ihinger, 2000). Our data shows that the mantle is not perfectly homogeneous for water concentrations and δD, but north of the Saint-Exupery fracture zone, we mainly observe homogeneous compositions, suggesting that the characteristic size of the heterogeneities is close to the characteristic mixing length along the ridge.

As illustrated by the $(La/Sm)_N$ ratio, our samples fall within the field of N-MORB. The gradual increase of $^{206}Pb/^{204}Pb$ ratio northwards illustrates the slightly higher amount of HIMU-type component in the source (Hamelin et al., 2010). Despite the two samples with the lowest $^{206}Pb/^{204}Pb$ (PAC1CV04 and PAC1DR12-1) also display low δD, there is no correlation

between δD and $(La/Sm)_N$ or $^{206}Pb/^{204}Pb$ (figure 9), so no enriched source with high $(La/Sm)_N$, δD and H_2O content can be infered, in contrast with observations near Iceland (Poreda et al., 1986) or along the Salas y Gomez seamount chain (Kingsley et al., 2002). This suggests than the heterogeneity in water contents and δD relates to a distinct process, and the lack of relationship with Pb-isotopes (seen as a tracer for a HIMU-type component) precludes the use of the δD variability to constrain the D/H ratio of the HIMU component.

The only apparent relationship is a negative correlation between δD and TiO_2/H_2O-ratios (figure 9), driven by two samples from the area south of the Saint Exupery fracture zone (PAC1CV04 and PAC1CV07). These two samples have the lowest H_2O/Ce of the sample suite (134 and 112), the lowest calculated H_2O_{source} and low δD (-76.6 and -69.6‰). Interestingly, their H_2O/TiO_2 and K_2O/TiO_2 are comparable to samples from the Siqueiros fracture zone (Saal et al., 2002, among others). These last two characteristics have been interpreted as resulting from a prior melting event of the source (Perfit et al., 1996; Danyushevsky et al., 2000; Cartigny et al., 2008), and their δD would suggest that the hydrogen left in the residue after partial melting is depleted in D. However, the apparent correlation is not significant if those two samples are not taken into account, as might be expected if the high TiO_2/H_2O ratios reflect a specific process.

Despite having little evidence for significant variability in major and trace elements, we investigate the possibility that the ranges in water content and δD observed reflect a heterogeneous source, containing two distinct components. Without making any a priori hypothesis on the characteristic size

or shape of the heterogeneities, we expect that for higher spreading rates, the more abundant production of basaltic liquids and the existence of more permanent magma chambers will lead to more homogeneous lavas erupted on the sea floor. If different water contents are assumed, the most water-rich component would be more fusible, and for low amounts of melting a second episode of melting would be necessary to express the characteristic water content and δD of the more refractory component. Samples PAC1CV04, CV06 and CV07 present low δD and low calculated water in the source, so this explanation looks promising, but we would expect samples with melting rate scaling to water content of the source. Yet the calculated melting rates range for a homogeneous mantle (with respect to major elements) is limited, only from 8 to 11% (figure 8), and previous studies do not suggest a major element concentration contrast in the southernmost section of the sampling area.

The size of possible heterogeneities is limited by the diffusion rate of hydrogen in the conditions of the upper mantle. For the fast axis of olivines at mantle temperatures, it is of the order of 10^{-8} $m^2.s^{-1}$ (Hercule and Ingrin, 1999; Ingrin, 2006). For residence times of 10^8 years, heterogeneities must be larger than 5 km, three orders of magnitude greater than the heterogeneities limit for trace elements (about 2 m, Allègre and Turcotte (1986)). This 5 km figure is smaller than the scale of sampling, although fracture zones can also play the role of barriers between different mantle domains.

So far, the lack of relationship between H_2O/Ce, δD and Pb isotopes suggest that for this sample suite, the variability observed cannot be accounted for by the presence of an uniquely defined component richer in water and/or

D and with a distinct $^{206}Pb/^{204}Pb$.

4.6. A reference zone for the study of the N-MORB source

Previous studies on the δD-values of N-MORB have mainly focused on samples from the north Atlantic and Pacific oceans (Kyser and O'Neil, 1984; Poreda et al., 1986; Pineau and Javoy, 1994; Pineau et al., 2004; Hauri et al., 2006b; Cartigny et al., 2008). These studies concluded that the uncontaminated N-MORB source had a δD of -80$\pm$10‰ (even if the average value measured in those studies is closer to -70‰). Most of those studies also used an extraction technique (induction-heating in Pt crucibles) which can cause biases of more than 10‰ (Clog et al., 2012). The recent study of (Bindeman et al., 2012), which does not use crucibles however, found the δD of Macquarie Island basalts to be close to -75$\pm$5‰. Although falling within the canonical mantle range, it must be noted that those samples are very enriched compared to N-MORB (La/Sm_N >1.3 for the most depleted one) and are therefore not representative of the depleted mantle.

N-MORB from the North Atlantic measured with the same protocol as in this study (Clog et al., 2012) have δD of $\approx$-60‰ and do not outline the existence of a distinct δD between the Pacific-Antarctic and the North Pacific or Atlantic mantles. Nonetheless, the dataset is still restricted and we are going to evaluate whether this part of the upper depleted mantle can plausibly have a distinct δD.

4.6.1. Geodynamic model

There are two ways to consider mantle water degassing flux at ridges. The first is that we observe degassing of some primordial water from the

upper mantle (as for Craig and Lupton (1976)). In this case the apparent contrast with the North Atlantic and North Pacific could be inherited from the processes of crust extraction. This proposition is however unlikely. First, the South Pacific, the North Atlantic and the North Pacific mantle domains have very similar e.g. Sr-isotopes compositions, suggesting an overall similar history and homogeneity resulting from mantle convection (van Keken et al., 2002; Hamelin et al., 2011, among others). Second, water is recycled in the mantle at subduction zones, which is likely to erase any primitive signature. This is illustrated by the high H_2O/Ce ratios in the North Atlantic due to recent rapid subduction (Michael, 1995) or by the distribution of δD observed in the Manus basin glasses (Shaw et al., 2012). It is thus unlikely that the southern Pacific mantle present a strong, inherited, δD contrast compared to the rest of the upper mantle.

The alternative, generally accepted model considers the hydrogen cycle as in equilibrium chemically and isotopically (steady state), with water recycled to the convecting mantle at subduction zones (Ito et al., 1983; Bebout, 1995; Williams and Hemley, 2001; Dixon et al., 2002). This is supported by the stable continental freeboard in the last half-billion years and analysis of old hydrated rocks (Galer, 1991; Lécuyer et al., 1998). Recent estimates range from 0.2 to 2 ocean masses contained in the mantle, (between 0.3 et 2.8 10^{24} g Bolfan-Casanova et al., 2000; Bolfan-Casanova, 2005; Javoy, 2005; Keppler, 2006; Hirschmann, 2006), with half in the transition zone and very little in the lower mantle (less than 5% of the total water, although this number depends on the oxygen fugacity of the lower mantle). The large range in mantle water budget reflects that several hypotheses are considered.

With the current ridge and hotspot water output (10^{14} g/an), the residence time is thus between 3 and 28 Gyr, but fluxes were probably greater during the Hadean and Archean and the equilibrium may have been reached early in Earth history. In this model, changing the composition of the upper mantle is possible by changing how recycling occurs, i.e., how much water is devolatilized, which P-T path the subducting slab follows, or depending on the thickness and extent of serpentinization, for the mantle domains of the South Pacific and North Atlantic.

It should be noted that we have few direct constraints on the inward flux of water in the mantle, and especially on its isotopic composition. The subducting slab must loose more than 80% of its water (Nadeau et al., 1993; Chaussidon and Jambon, 1994; Dixon et al., 2002) to the arc system, and for the Pacific ocean, flux towards the mantle wedges is not relevant as the subduction zones are directed outwards. The water content of the hydrated oceanic crust is between 0.5 and 5% with a δD between -30 and -50‰ (Kawahata et al., 1987; Kusakabe et al., 1989; Agrinier et al., 1995; Shilobreeva et al., 2011), but the sampling is very sparse, especially with respect to depth, and the hydration of the lower oceanic lithosphere is hard to constrain (Rüpke et al., 2004). To reach isotopic equilibrium of the water cycle, the final average δD of slabs after dehydration should be equal to the average δD of the ridges flux (e.g. -60‰ as measured in this study), but studies have given possible ranges from -30 to - 200‰ for effectively recycled hydrogen (Kingsley et al., 2002; Shaw et al., 2008, 2012).

4.6.2. Changing the δD of the slab

The first obvious answer to obtain a higher δD is to increase the δD of the recycled crust before dehydration, either with a different δD of the ocean or by changing the average temperature of alteration. Both are extremely unlikely for the following reasons.

The first is at odds with results on Phanerozoic and Proterozoic ophiolites suggesting little variability of oceans δD values (Lécuyer et al., 1998). It would also require, for a difference between the north and south Pacific to be apparent today, that the recycling timescale differs markedly between the different mantle domains.

The second would require a hydrothermal alteration temperature several hundreds of degrees higher (Suzuoki and Epstein, 1976) than the one which produces the altered crust studied by Kawahata et al. (1987); Kusakabe et al. (1989); Agrinier et al. (1995). There is at present no compelling argument suggesting that oceanic basalts could have been altered at such higher temperatures. Moreover, given that present hydration of the ocean crust depends upon spreading rate, it is worth noting that there is again no evidence for significant change in spreading rate at least since 180 Ma (Cogné and Humler, 2004).

4.6.3. Subduction processes

The H_2O/Ce ratios on the two supersegments studied here (186±30 and 173±15) are similar to those measured in the rest of the Pacific ridges system (between 150 and 220, Michael (1995); Le Roux et al. (2006)). A smaller extent of dehydration during subduction is therefore not a possible explanation for the apparent North Pacific/South Pacific δD contrast. Nevertheless,

the exact P-T path followed by the slab depends on the dipping angle of the subduction zone (Hager and O'connell, 1978; Cahill and Isacks, 1992). This could be critical for the final δD of the slab, as destabilisation of the water-bearing minerals will occur at different pressures and temperatures (Schmidt and Poli, 1998; Kawamoto, 2006; Smyth, 2006). Water solubility in nomimally anhydrous minerals depends on the pressure, so even for the same amount of dehydration (Kohlstedt et al., 1996; Mierdel et al., 2007), the final δD could differ. Indeed, even at 900°C, fractionation of hydrogen isotopes between minerals is significant (up to 10‰ : Suzuoki and Epstein, 1976; Graham et al., 1984; Dobson et al., 1989; Vennemann and O'Neil, 1996). This type of scenario would also create differences for other fluid-mobile elements like Li and B, and could explain the small differences between the two supersegments ($\overline{\delta \mathrm{D}} \approx$ -63‰ in the south and $\overline{\delta \mathrm{D}} \approx$ -58‰ in the north).

Yet this scenario can hardly lead to the 20‰ contrast between our results and those of Kyser and O'Neil (1984). If we model the slab dehydration as an open-system loss of water, the average fractionation of water would need to differ by 10‰. Experiments on fractionation factors between water and hydrated minerals indicate that it corresponds to a ≈150°C change in the range 500-900°C (Suzuoki and Epstein, 1976). This explanation is therefore not satisfactory with the current view of P-T paths and and dehydration of recycled ocean crust.

4.6.4. Revising the δD of the upper depleted mantle

We have shown that previous measurements could suffer from an experimental bias (Clog et al., 2012), and have not been able to find a satisfactory scenario explaining why the south Pacific would be enriched in D compared

to previous data and other locations while being otherwise a perfect example of the upper depleted mantle, unaffected by mantle plumes. Our view is therefore that slight variations in δD (and H_2O/Ce) can be produced by dehydration and recycling of water, but that the large contrast with previous data reflects analytical artifacts.

This sample suite presents many advantages to characterize the isotopic composition of the depleted mantle. Previous researchers have shown that the source composition is typical of the depleted mantle with limited and gradual variations in compositions in the area. Most of the variations are due to igneous processes, and the variation in spreading rate and ridge structure strengthen the conclusion that contamination is not a major obstacle to the determination of hydrogen isotopic composition of the source of N-MORB. Finally, the high number of samples (40 in this area compared to less than 70 N-MORB measured in a variety of locations in the literature, Craig and Lupton (1976); Satake and Matsuda (1979); Kyser and O'Neil (1984); Poreda et al. (1986); Chaussidon et al. (1991); Pineau and Javoy (1994); Kingsley et al. (2002); Pineau et al. (2004); Cartigny et al. (2008)) limits the possibility of sample bias when calculating averages.

On the basis of this study, we propose that the average δD of the upper depleted mantle is rather -60$\pm$5‰. Although the same average value and a similar range were observed on 8 N-MORB from the Middle Atlantic Ridge (Clog et al., 2012), further studies on other ridges are necessary to confirm this figure. Variations observed in isotopic composition and water content shows that the upper mantle is not homogeneous, but present both small scales heterogeneities which are averaged by melts pooling when the

spreading rate is higher than 7 cm/year, and zonations at a larger scale leading to different average values on the northern and southern supersegments, illustrating the distribution of heterogeneities in the convecting mantle.

5. Conclusions

Despite widespread Cl contamination, assimilation of seawater-derived fluids or interaction with hydrated rocks did not significantly affect concentrations or isotopic compositions of hydrogen for our suite of samples. An increase in Cl contamination with spreading rate was observed. All samples are N-MORB with no evidence of influence from hotspots. Samples were undersaturated with respect to H_2O, and variations in concentrations of water are mainly due to igneous processes. The water content in the source ranges from 150 to 250 ppm. The average δD are -63 and -58‰ and the water to cerium ratios of 186±30 and 173±15 for the southern and northern supersegments respectively. This apparent enrichment compared to previous studies (δD≈-70‰) is not due to difference during the recycling of water. It is rather explained by a combination of a potential experimental bias and different interpretation on the influence of contamination. The δD of the upper depleted mantle is close to -60±5‰, with variations in δD and H_2O/Ce at different length scales resulting from recycling and ridge processes.

ACKNOWLEDGMENTS

The LSCE provided the water standards used for this study. We wish to thank Michel Fialin for his assitance in performing the chlorine content measurements, Manuel Moreira for access to the PACANTARCTIC2 samples

and Cédric Hamelin for early access to geochemical data on those samples. We acknowledge support from the CNRS via its SEDIT research program. This is IPGP contribution number XX-XXXX.

References

Agrinier, P., Hékinian, R., Bideau, D., Javoy, M., 1995. O and H stable isotope compositions of oceanic crust and upper mantle rocks exposed in the Hess Deep near the Galapagos Triple Junction. Earth and Planetary Science Letters 136 (3-4), 183 – 196.

Allègre, C., Turcotte, D., 1986. Implications of a two-component marble-cake mantle. Nature 323 (6084), 123–127.

Asimow, P. D., Langmuir, C. H., 2003. The importance of water to oceanic mantle melting regimes. Nature 421 (6925), 815–820.

Aubaud, C., Hauri, E. H., Hirschmann, M. M., 2004. Hydrogen partition coefficients between nominally anhydrous minerals and basaltic melts. Geophysical Research Letters 31, L20611.

Bebout, G. E., 1995. The impact of subduction-zone metamorphism on mantle-ocean chemical cycling. Chemical Geology 126 (2), 191–218.

Bell, D. R., Ihinger, P. D., 2000. The isotopic composition of hydrogen in nominally anhydrous mantle minerals. Geochimica et Cosmochimica Acta 64 (12), 2109–2118.

Berndt, M., Seal, R., Shanks III, W., Seyfried Jr, W., 1996. Hydrogen isotope systematics of phase separation in submarine hydrothermal systems: ex-

perimental calibration and theoretical models. Geochimica et Cosmochimica Acta 60 (9), 1595–1604.

Bézos, A., Humler, E., 2005. The $Fe^{3+}/\Sigma Fe$ ratios of MORB glasses and their implications for mantle melting. Geochimica et Cosmochimica Acta 69 (3), 711–725.

Bigeleisen, J., Perlman, M. L., Prosser, H. C., 1952. Conversion of hydrogenic materials to hydrogen for isotopic analysis. Analytical Chemistry 24 (8), 1356–1357.

Bindeman, I. N., Kamenetsky, V. S., Palandri, J., Vennemann, T., 2012. Hydrogen and oxygen isotope behaviors during variable degrees of upper mantle melting: Example from the basaltic glasses from macquarie island. Chemical Geology 310311, 126 – 136.

Bolfan-Casanova, N., 2005. Water in the earth's mantle. Mineral Mag 69 (3), 229–257.

Bolfan-Casanova, N., Keppler, H., Rubie, D. C., 2000. Water partitioning between nominally anhydrous minerals in the MgO-SiO_2-H_2O system up to 24 GPa: implications for the distribution of water in the earth's mantle. Earth and Planetary Science Letters 182 (3-4), 209–221.

Bonifacie, M., Jendrzejewski, N., Agrinier, P., Humler, E., Coleman, M., Javoy, M., 2008. The chlorine isotope composition of Earth's mantle. Science 319 (5869), 1518.

Cahill, T., Isacks, B. L., 1992. Seismicity and shape of the subducted Nazca plate. Journal of Geophysical Research 97 (B12), PP. 17,503–17,529.

Cartigny, P., Pineau, F., Aubaud, C., Javoy, M., 2008. Towards a consistent mantle carbon flux estimate: Insights from volatile systematics (H_2O/Ce, δD, CO_2/Nb) in the North Atlantic mantle (14°N and 34°N). Earth and Planetary Science Letters 265 (3-4), 672–685.

Castillo, P. R., Natland, J. H., Niu, Y., Lonsdale, P. F., 1998. Sr, Nd and Pb isotopic variation along the Pacific-Antarctic risecrest, 53-57°S: implications for the composition and dynamics of the South Pacific upper mantle. Earth and Planetary Science Letters 154 (1-4), 109–125.

Chaussidon, M., Jambon, A., 1994. Boron content and isotopic composition of oceanic basalts: Geochemical and cosmochemical implications. Earth and Planetary Science Letters 121 (3-4), 277–291.

Chaussidon, M., Sheppard, S. M. F., Michard, A., 1991. Hydrogen, sulphur and neodymium isotope variations in the mantle beneath the EPR at 12°50'N. In: Stable isotope geochemistry: a tribute to Samuel Epstein, Geochemical Society Special Publication Edition. Taylor, H.P., O'Neil, J.R., Kaplan, I.R. (Eds), pp. 325–337.

Clog, M., Cartigny, P., Aubaud, C., 2012. Experimental evidence for interaction of water vapor and platinum crucibles at high temperatures: Implications for volatiles from igneous rocks and minerals. Geochimica et Cosmochimica Acta 83 (1), 125–137.

Cogné, J., Humler, E., 2004. Temporal variation of oceanic spreading and crustal production rates during the last 180 my. Earth and Planetary Science Letters 227 (3), 427–439.

633 Craig, H., Lupton, J. E., 1976. Primordial neon, helium, and hydrogen in
634 oceanic basalts. Earth and Planetary Science Letters 31 (3), 369–385.

635 Danyushevsky, L. V., Eggins, S. M., Falloon, T., Christie, D., 2000. H_2O
636 abundance in depleted to moderately enriched mid-ocean ridge magmas;
637 part I: Incompatible behaviour, implications for mantle storage, and origin
638 of regional variations. J. Petrology 41 (8), 1329–1364.

639 DeMets, C., Gordon, R. G., Argus, D. F., Stein, S., 1990. Current plate
640 motions. Geophysical Journal International 101 (2), 425–478.

641 Dixon, J., Clague, D., 2001. Volatiles in basaltic glasses from Loihi seamount,
642 Hawaii: evidence for a relatively dry plume component. Journal of Petrol-
643 ogy 42 (3), 627–654.

644 Dixon, J., Leist, L., Langmuir, C., Schilling, J., 2002. Recycled dehydrated
645 lithosphere observed in plume-influenced mid-ocean-ridge basalt. Nature
646 420, 385–389.

647 Dixon, J., Stolper, E., 1995. An experimental study of water and carbon
648 dioxide solubilities in mid-ocean ridge basaltic liquids. Part II: applications
649 to degassing. Journal of Petrology 36 (6), 1633.

650 Dobson, P. F., Epstein, S., Stolper, E. M., 1989. Hydrogen isotope frac-
651 tionation between coexisting vapor and silicate glasses and melts at low
652 pressure. Geochimica et Cosmochimica Acta 53 (10), 2723–2730.

653 Galer, S., 1991. Interrelationships between continental freeboard, tectonics
654 and mantle temperature. Earth and Planetary Science Letters 105 (1-3),
655 214 – 228.

Géli, L., Aslanian, D., Olivet, J., Vlastelic, I., Dosso, L., Guillou, H., Bougault, H., 1998. Location of Louisville hotspot and origin of Hollister ridge: geophysical constraints. Earth and Planetary Science Letters 164 (1-2), 31–40.

Graham, C., Harmon, R., Sheppard, S., 1984. Experimental hydrogen isotope studies: hydrogen isotope exchange between amphibole and water. American Mineralogist 69, 128–138.

Grant, K. J., Kohn, S. C., Brooker, R. A., 2007. The partitioning of water between olivine, orthopyroxene and melt synthesised in the system albite-forsterite-H_2O. Earth and Planetary Science Letters 260 (1-2), 227–241.

Hager, B. H., O'connell, R. J., 1978. Subduction zone dip angles and flow driven by plate motion. Tectonophysics 50 (2-3), 111–133.

Hamelin, C., Dosso, L., Hanan, B., Barrat, J., Ondréas, H., 2010. Sr-Nd-Hf isotopes along the Pacific Antarctic Ridge from 41 to 53°S. Geophysical Research Letters 37, L10303.

Hamelin, C., Dosso, L., Hanan, B., Moreira, M., Kositsky, A., Thomas, M., 2011. Geochemical portray of the pacific ridge: New isotopic data and statistical techniques. Earth and Planetary Science Letters 302 (1), 154–162.

Hauri, E., Gaetani, G., Green, T., 2006a. Partitioning of water during melting of the earth's upper mantle at H_2O-undersaturated conditions. Earth and Planetary Science Letters 248 (3-4), 715–734.

Hauri, E., Shaw, A., Wang, J., Dixon, J., King, P., Mandeville, C., 2006b. Matrix effects in hydrogen isotope analysis of silicate glasses by SIMS. Chemical Geology 235 (3-4), 352–365.

Hercule, S., Ingrin, J., 1999. Hydrogen in diopside; diffusion, kinetics of extraction-incorporation, and solubility. American Mineralogist 84 (10), 1577–1587.

Hirschmann, M. M., 2006. Water, melting, and the deep earth H_2O cycle. Annual Review of Earth and Planetary Sciences 34 (1), 629–653.

Ingrin, J., 2006. Diffusion of hydrogen in minerals. Reviews in Mineralogy and Geochemistry 62 (1), 291–320.

Ito, E., Harris, D. M., Anderson, A. T., 1983. Alteration of oceanic crust and geologic cycling of chlorine and water. Geochimica et Cosmochimica Acta 47 (9), 1613–1624.

Jambon, A., Déruelle, B., Dreibus, G., Pineau, F., 1995. Chlorine and bromine abundance in MORB: the contrasting behaviour of the Mid-Atlantic ridge and East Pacific Rise and implications for chlorine geodynamic cycle. Chemical Geology 126 (2), 101–117.

Jambon, A., Zimmermann, J., 1990. Water in oceanic basalts: evidence for dehydration of recycled crust. Earth and Planetary Science Letters 101 (2-4), 323–331.

Javoy, M., 2005. Where do the oceans come from? Comptes Rendus Géoscience 337 (1-2), 139–158, colloquium on Continental Waters, Paris, FRANCE, SEP 15-17, 2003.

Jendrzejewski, N., Javoy, M., Trull, T., 1996. Mesures quantitatives de carbone et d'eau dans les verres basaltiques naturels par spectroscopie infrarouge. partie II: l'eau= quantitative measurements of water and carbon concentrations in natural basaltic glasses by infrared spectroscopy. part II: water. Comptes rendus de l'Académie des sciences. Série 2. Sciences de la terre et des planètes 322 (9), 735–742.

Kamenetsky, V. S., Eggins, S. M., 2012. Systematics of metals, metalloids, and volatiles in MORB melts: Effects of partial melting, crystal fractionation and degassing (a case study of Macquarie island glasses). Chemical Geology 302303 (0), 76–86.

Kawahata, H., Kusakabe, M., Kikuchi, Y., 1987. Strontium, oxygen, and hydrogen isotope geochemistry of hydrothermally altered and weathered rocks in DSDP hole 504B, Costa Rica rift. Earth and Planetary Science Letters 85 (4), 343–355.

Kawamoto, T., 2006. Hydrous phases and water transport in the subducting slab. Reviews in Mineralogy and Geochemistry 62 (1), 273–289.

Kelley, K., Cottrell, E., 2009. Water and the oxidation state of subduction zone magmas. Science 325 (5940), 605–607.

Kelley, K. A., Plank, T., Grove, T. L., Stolper, E. M., Newman, S., Hauri, E., 2006. Mantle melting as a function of water content beneath back-arc basins. Journal of Geophysical Research (Solid Earth) 111, B09208.

Kendrick, M., Kamenetsky, V., Phillips, D., Honda, M., 2012. Halogen sys-

tematics (Cl, Br, I) in Mid-Ocean Ridge Basalts: A Macquarie Island case study. Geochimica et Cosmochimica Acta 81 (7), 82–93.

Kent, A. J., Clague, D. A., Honda, M., Stolper, E. M., Hutcheon, I. D., Norman, M. D., 1999a. Widespread assimilation of a seawater-derived component at Loihi seamount, Hawaii. Geochimica et Cosmochimica Acta 63 (18), 2749–2761.

Kent, A. J. R., Norman, M. D., Hutcheon, I. D., Stolper, E. M., 1999b. Assimilation of seawater-derived components in an oceanic volcano: evidence from matrix glasses and glass inclusions from Loihi seamount, Hawaii. Chemical Geology 156 (1-4), 299–319.

Keppler, H., 2006. Thermodynamics of water solubility and partitioning. Reviews in Mineralogy and Geochemistry 62 (1), 193–230.

Kingsley, R., Schilling, J., Dixon, J., Swart, P., Poreda, R., Simons, K., 2002. D/H ratios in basalt glasses from the Salas y Gomez mantle plume interacting with the East Pacific Rise: water from old D-rich recycled crust or primordial water from the lower mantle? Geochem. Geophys. Geosyst 3 (4), 1025.

Klein, E. M., Langmuir, C. H., 1987. Global correlations of ocean ridge basalt chemistry with axial depth and crustal thickness. Journal of Geophysical Research 92 (B8), PP. 8089–8115.

Klingelhoefer, F., Ondréas, H., Briais, A., Hamelin, C., Dosso, L., 2006. New structural and geochemical observations from the Pacific-Antarctic

ridge between 52°45'S and 41°15'S. Geophysical Research Letters 33 (21), L21312.

Kohlstedt, D. L., Keppler, H., Rubie, D. C., 1996. Solubility of water in the α ,β and γ phases of $(Mg,Fe)_2SiO_4$. Contributions to Mineralogy and Petrology 123 (4), 345–357.

Kohn, S. C., 2006. The partitioning of water between nominally anhydrous minerals and silicate melts. Reviews in Mineralogy and Geochemistry 62 (1), 231–241.

Kusakabe, M., Shibata, T., Yamamoto, M., Mayeda, S., Kagami, H., Honma, H., Masuda, H., Sakai, H., 1989. Petrology and isotope characteristics (H, o, s, sr, and nd) of basalts from Ocean Drilling Program hole 504B, leg 111, Costa Rica Rift. In: Becker, K., Sakai, H., et al., Proc. ODP, Sci. Results. Vol. 111. pp. 47–60.

Kyser, T., O'Neil, J. R., 1984. Hydrogen isotope systematics of submarine basalts. Geochimica et Cosmochimica Acta 48 (10), 2123 – 2133.

Langmuir, C. H., Bender, J. F., 1984. The geochemistry of oceanic basalts in the vicinity of transform faults: Observations and implications. Earth and Planetary Science Letters 69 (1), 107–127.

Le Roux, P., Shirey, S., Hauri, E., Perfit, M., Bender, J., 2006. The effects of variable sources, processes and contaminants on the composition of northern EPR MORB (8–10°N and 12–14°N): evidence from volatiles (H_2O, CO_2, S) and halogens (F, Cl). Earth and Planetary Science Letters 251 (3-4), 209–231.

768 Lécuyer, C., Gillet, P., Robert, F., 1998. The hydrogen isotope composition
769 of seawater and the global water cycle. Chemical Geology 145 (3-4), 249–
770 261.

771 Lehnert, K., Su, Y., Langmuir, C., Sarbas, B., Nohl, U., 2000. A global geo-
772 chemical database structure for rocks. Geochemistry Geophysics Geosys-
773 tems 1 (5), 1012–14.

774 McDonough, W. F., Sun, S., 1995. The composition of the earth. Chemical
775 Geology 120 (3-4), 223–253.

776 Michael, P., 1995. Regionally distinctive sources of depleted MORB: evidence
777 from trace elements and H_2O. Earth and Planetary Science Letters 131 (3-
778 4), 301–320.

779 Michael, P. J., Cornell, W. C., 1998. Influence of spreading rate and magma
780 supply on crystallization and assimilation beneath mid-ocean ridges: Ev-
781 idence from chlorine and major element chemistry of mid-ocean ridge
782 basalts. Journal of Geophysical Research 103 (B8), PP. 18,325–18,356.

783 Mierdel, K., Keppler, H., Smyth, J. R., Langenhorst, F., 2007. Water solu-
784 bility in aluminous orthopyroxene and the origin of earth's asthenosphere.
785 Science 315 (5810), 364–368.

786 Moreira, M. A., Dosso, L., Ondréas, H., 2008. Helium isotopes on the Pacific-
787 Antarctic ridge (52.5°–41.5°S). Geophysical Research Letters 35 (10),
788 L10306.

789 Nadeau, S., Philippot, P., Pineau, F., 1993. Fluid inclusion and mineral iso-
790 topic compositions (H-C-O) in eclogitic rocks as tracers of local fluid mi-

791 gration during high-pressure metamorphism. Earth and Planetary Science
792 Letters 114 (4), 431–448.

793 Perfit, M., Fornari, D., Ridley, W., Kirk, P., Casey, J., Kastens, K., Reynolds,
794 J., Edwards, M., Desonie, D., Shuster, R., et al., 1996. Recent volcanism in
795 the Siqueiros transform fault: picritic basalts and implications for MORB
796 magma genesis. Earth and Planetary Science Letters 141 (1), 91–108.

797 Pineau, F., Javoy, M., 1994. Strong degassing at ridge crests: The behaviour
798 of dissolved carbon and water in basalt glasses at 14°N, Mid-Atlantic ridge.
799 Earth and Planetary Science Letters 123 (1-3), 179–198.

800 Pineau, F., Shilobreeva, S., Hékinian, R., Bideau, D., Javoy, M., 2004. Deep-
801 sea explosive activity on the Mid-Atlantic ridge near 34°50' N: a stable
802 isotope (C, H, O) study. Chemical Geology 211 (1-2), 159–175.

803 Poreda, R., Schilling, J., Craig, H., 1986. Helium and hydrogen isotopes
804 in ocean-ridge basalts north and south of Iceland. Earth and Planetary
805 Science Letters 78 (1), 1–17.

806 Rüpke, L. H., Morgan, J. P., Hort, M., Connolly, J. A. D., 2004. Serpentine
807 and the subduction zone water cycle. Earth and Planetary Science Letters
808 223 (1-2), 17 – 34.

809 Saal, A. E., Hauri, E. H., Langmuir, C. H., Perfit, M. R., 2002. Vapour un-
810 dersaturation in primitive mid-ocean-ridge basalt and the volatile content
811 of earth's upper mantle. Nature 419 (6906), 451–455.

812 Satake, H., Matsuda, J., 1979. Strontium and hydrogen isotope geochemistry

of fresh and metabasalt dredged from the Mid-Atlantic ridge. Contributions to Mineralogy and Petrology 70 (2), 153–157.

Schmidt, M. W., Poli, S., 1998. Experimentally based water budgets for dehydrating slabs and consequences for arc magma generation. Earth and Planetary Science Letters 163 (1-4), 361–379.

Shaw, A., Hauri, E., Behn, M., Hilton, D., Macpherson, C., Sinton, J., 2012. Long-term preservation of slab signatures in the mantle inferred from hydrogen isotopes. Nature Geoscience 5 (3), 224–228.

Shaw, A. M., Hauri, E. H., Fischer, T. P., Hilton, D. R., Kelley, K. A., 2008. Hydrogen isotopes in Mariana arc melt inclusions: Implications for subduction dehydration and the deep-Earth water cycle. Earth and Planetary Science Letters 275 (1-2), 138–145.

Shilobreeva, S., Martinez, I., Busigny, V., Agrinier, P., Laverne, C., 2011. Insights into c and h storage in the altered oceanic crust: Results from odp/iodp hole 1256d. Geochimica et Cosmochimica Acta 75 (9), 2237–2255.

Smyth, J. R., 2006. Hydrogen in high pressure silicate and oxide mineral structures. Reviews in Mineralogy and Geochemistry 62 (1), 85–115.

Soule, S. A., Fornari, D. J., Perfit, M. R., Ridley, W. I., Reed, M. H., Cann, J. R., 2006. Incorporation of seawater into mid-ocean ridge lava flows during emplacement. Earth and Planetary Science Letters 252 (3-4), 289–307.

Sours-Page, R., Johnson, K., Nielsen, R., Karsten, J., 1999. Local and regional variation of MORB parent magmas: evidence from melt inclusions

836 from the Endeavour segment of the Juan de Fuca ridge. Contributions to
837 mineralogy and petrology 134 (4), 342–363.

838 Suzuoki, T., Epstein, S., 1976. Hydrogen isotope fractionation between OH-
839 bearing minerals and water. Geochimica et Cosmochimica Acta 40 (10),
840 1229–1240.

841 van Keken, P., Hauri, E., Ballentine, C., 2002. Mantle mixing: the generation,
842 preservation, and destruction of chemical heterogeneity. Annual Review of
843 Earth and Planetary Sciences 30 (1), 493–525.

844 Vennemann, T., O'Neil, J., 1993. A simple and inexpensive method of hy-
845 drogen isotope and water analyses of minerals and rocks based on zinc
846 reagent. Chemical Geology 103 (1-4), 227 – 234.

847 Vennemann, T., O'Neil, J. R., 1996. Hydrogen isotope exchange reactions
848 between hydrous minerals and molecular hydrogen: I. a new approach for
849 the determination of hydrogen isotope fractionation at moderate temper-
850 atures. Geochimica et Cosmochimica Acta 60 (13), 2437–2451.

851 Vlastélic, I., Aslanian, D., Dosso, L., Bougault, H., Olivet, J. L., Geli, L.,
852 1999. Large-scale chemical and thermal division of the Pacific mantle. Na-
853 ture 399 (6734), 345–350.

854 Vlastélic, I., Dosso, L., Bougault, H., Aslanian, D., Géli, L., Etoubleau,
855 J., Bohn, M., Joron, J. L., Bollinger, C., 2000. Chemical systematics of
856 an intermediate spreading ridge: the Pacific–Antarctic ridge between 56
857 degrees s and 66 degrees s. J. Geophys. Res. Solid Earth 105, 2915–2936.

858 Vlastélic, I., Dosso, L., Guillou, H., Bougault, H., Geli, L., Etoubleau, J.,
859 Joron, J., 1998. Geochemistry of the Hollister ridge: relation with the
860 Louisville hotspot and the Pacific-Antarctic ridge. Earth and Planetary
861 Science Letters 160 (3-4), 777–793.

862 Weaver, J. S., Langmuir, C. H., 1990. Calculation of phase equilibrium in
863 mineral-melt systems. Computers & Geosciences 16 (1), 1–19.

864 Williams, Q., Hemley, R. J., 2001. Hydrogen in the deep earth. Annual Re-
865 view of Earth and Planetary Sciences 29 (1), 365–418.

6. TABLES

Table 1: Previous data for the southern supersegment : major elements (Vlastélic et al., 2000) and segment number.

	SiO_2	Al_2O_3	FeO	MnO	MgO	CaO	Na_2O	K_2O	TiO_2	Total	Segment
PAC1 CV1	49.78	15.70	9.79	0.18	8.45	11.71	2.49	0.04	1.10	99.24	1
PAC1 CV2	50.78	14.37	10.49	0.19	7.74	11.25	2.55	0.06	1.67	99.10	1
PAC1 CV3	50.70	15.53	8.60	0.16	8.57	11.91	2.53	0.08	1.20	99.28	1
PAC1 CV4	50.30	15.46	8.55	0.16	8.78	12.32	2.46	0.04	1.05	99.12	1
PAC1 CV6	50.44	15.37	9.31	0.17	8.51	12.01	2.50	0.04	1.23	99.58	1
PAC1 CV7	51.06	14.50	9.80	0.19	7.88	12.03	2.71	0.04	1.31	99.52	1
PAC1 DR3	51.18	14.51	9.88	0.18	7.30	11.21	3.00	0.15	1.59	99.00	2
PAC1 DR4	49.13	15.71	10.08	0.18	7.25	11.83	2.87	0.12	1.35	98.52	3
PAC1 DR5-1	51.00	15.45	8.42	0.15	8.33	12.01	2.82	0.09	1.19	99.46	4
PAC1 DR6	50.99	13.99	11.20	0.20	6.93	10.58	2.86	0.12	2.02	98.89	4
PAC1 DR7-1	50.75	14.43	10.70	0.22	6.83	10.58	3.03	0.19	1.94	98.67	4
PAC1 DR7-2	50.83	14.43	10.52	0.18	7.35	11.29	2.91	0.12	1.69	99.32	4
PAC1 DR9	50.75	13.42	12.15	0.22	6.36	10.44	3.09	0.12	2.20	98.75	5
PAC1 DR10-1	53.79	14.10	10.77	0.21	4.83	8.59	3.43	0.48	1.73	97.93	5
PAC1 DR10-2	51.46	14.10	10.87	0.20	6.22	10.36	3.37	0.25	1.75	98.58	5
PAC1 DR11-1	50.21	14.32	9.25	0.17	7.33	11.34	2.70	0.06	1.31	96.69	6
PAC1 DR12-1	50.94	15.62	8.49	0.15	8.85	12.31	2.32	0.03	1.03	99.74	6
PAC1 DR13-1	50.37	14.60	10.89	0.18	7.38	10.76	2.82	0.09	1.64	98.73	6
PAC1 DR13-2	50.50	14.52	11.01	0.19	7.42	10.73	2.85	0.09	1.65	98.96	6

Table 2: Previous data for the northern supersegment : major elements (Hamelin et al., 2010) and segment names.

	SiO_2	Al_2O_3	FeO	MnO	MgO	CaO	Na_2O	K_2O	TiO_2	Total	Segment
PAC2 DR 1-1	50.20	14.60	10.75	0.18	7.30	11.90	2.82	0.20	1.58	99.53	S1
PAC2 DR3-1											S1
PAC2 DR4-2	50.40	14.28	11.70	0.20	7.08	11.20	2.83	0.12	1.79	99.60	S1
PAC2 DR5-2	49.90	13.65	13.45	0.22	6.52	10.40	2.74	0.18	2.13	99.19	S2
PAC2 DR6-6	51.30	12.56	15.70	0.26	4.34	8.66	3.46	0.31	2.88	99.47	S2
PAC2 DR7-2											S3
PAC2 DR8-1	49.40	14.40	12.65	0.20	7.05	11.70	2.87	0.20	1.66	100.13	S3
PAC2 DR20-1	51.15	13.90	14.20	0.24	4.60	9.35	3.34	0.25	2.40	99.43	N1
PAC2 DR21-2	50.30	13.88	12.50	0.21	6.73	11.10	2.79	0.15	2.00	99.66	N1
PAC2 DR22-1	49.90	14.60	11.70	0.20	7.25	11.60	2.78	0.17	1.87	100.07	N1
PAC2 DR28-2	49.70	15.00	11.15	0.19	7.85	12.10	2.52	0.08	1.39	99.98	N3
PAC2 DR29-1	49.90	13.37	13.80	0.23	6.16	10.75	2.83	0.19	2.31	99.54	N3
PAC2 DR30-1	50.00	14.05	12.45	0.21	7.00	11.70	2.64	0.17	1.94	100.16	N3
PAC2 DR31-3	49.85	14.70	11.70	0.19	7.55	11.45	2.56	0.10	1.74	99.83	N3
PAC2 DR32-1	50.50	14.00	12.60	0.21	6.80	11.10	2.84	0.16	2.02	100.23	N4
PAC2 DR33-1	50.20	13.90	12.80	0.21	6.63	10.95	2.84	0.15	2.10	99.78	N4
PAC2 DR34-1	50.00	15.10	10.44	0.18	8.00	12.08	2.60	0.06	1.30	99.76	N4
PAC2 DR35-1a	49.50	13.15	15.05	0.23	5.65	9.93	3.05	0.17	2.93	99.66	N5
PAC2 DR36-1	49.60	14.25	12.50	0.20	7.07	11.30	2.80	0.15	2.09	99.96	N5
PAC2 DR37-2											N5
PAC2 DR38-1	49.10	15.7	10.80	0.18	8.35	11.70	2.67	0.09	1.42	99.72	N6

Table 3: Data table for the southern supersegment : K_2O, La and Sm content from Vlastélic et al. (2000); H_2O, Cl, Ce and δD from this study.

	Long. (°W)	Lat. (°S)	Depth (m)	H_2O (ppm)	δD (‰)	Cl (ppm)	Ce (ppm)	H_2O/Ce	$(La/Sm)_N$	Cl/K
PAC1 CV1	173.75	-65.10	2863	1192	-63.2	56	5.6	213	0.49	0.169
PAC1 CV2	172.43	-64.83	2936	2070	-60.5	61	10.5	197	0.47	0.122
PAC1 CV3	171.88	-64.53	2576	2217	-54.5	55	8.7	255	0.64	0.083
PAC1 CV4	169.40	-64.40	2340	844	-76.6	52	6.3	134	0.49	0.157
PAC1 CV6	166.06	-63.45	2755	1030	-65.7	53	5.2	198	0.44	0.160
PAC1 CV7	165.96	-63.54	1603	1182	-69.5	218	10.5	113	0.85	0.656
PAC1 DR3	156.08	-62.32	2219	2672	-66.4	175	14.8	181	0.84	0.140
PAC1 DR4	153.04	-62.41	1587	2151	-66.5	29	10.7	201	0.65	0.029
PAC1 DR5-1	154.54	-62	2344	1585	-61.3	43	10.2	155	0.77	0.058
PAC1 DR6	153.21	-60.94	2527	2705	-71.7	39	14.6	185	0.61	0.039
PAC1 DR7-1	152.08	-60	2362	3112	-60.8	533	17.9	174	0.76	0.338
PAC1 DR7-2	152.08	-60	2362	2437	-66.0	206	13.1	186	0.63	0.207
PAC1 DR9	149.14	-58.85	2484	2956	-65.2	380	15.9	186	0.56	0.381
PAC1 DR10-1	148.50	-57.89	2319	7808	-58.1	2395	39.6	197	0.94	0.601
PAC1 DR10-2	148.50	-57.89	2319	3835	-57.7	1008	23.1	166	0.80	0.485
PAC1 DR11-1	146.80	-57.63	2500	1889	-48.7	162	9.6	197	0.56	0.325
PAC1 DR12-1	146.29	-57.18	2539	1175	-69.0	48	6.0	196	0.45	0.193
PAC1 DR13-1	145.74	-56.57	2674	2112	-56.1	76	11.7	181	0.54	0.102
PAC1 DR13-2	145.74	-56.57	2674	2345	-65.4	66	11.1	211	0.61	0.088

Table 4: Data table for the northern supersegment. K_2O, La, Sm and Ce from Hamelin et al. (2010); H_2O. Cl and δD from this study.

	Long. (°W)	Lat. (°S)	Depth (m)	H_2O (ppm)	δD (‰)	Cl (ppm)	Ce (ppm)	H_2O/Ce	$(La/Sm)_N$	Cl/K
PAC2 DR 1-1	118.4	-52.52	2323	2397	-60.1	256	14.4	166.47	0.78556	0.154
PAC2 DR3-1	118.0	-51.79	2396	2783	-59.8	309	13.6	205.21		
PAC2 DR4-2	117.8	-51.42	2409	2310	-64.8	257	12.8	180.67	0.60379	0.258
PAC2 DR5-2g	117.4	-50.98	2784	3296	-60.9	309	17.6	186.92	0.81617	0.207
PAC2 DR6-6	117.2	-50.70	2610	6546	-51.2	78	39.0	168.01	0.86064	0.030
PAC2 DR7-2g	117.1	-50.24	2229	2764	-58.4	479				
PAC2 DR8-1	117.0	-49.99	2220	3012	-51.8	271	15.8	190.61	0.90177	0.163
PAC2 DR20-1	113.8	-49.73	2440	4797	-55.2	1631	34.2	140.34	0.80392	0.786
PAC2 DR21-2	113.6	-49.26	2338	2384	-56.2	308	14.0	170.82	0.65922	0.247
PAC2 DR22-1	113.4	-48.73	2413	2646	-56.6	348	14.6	180.83	0.60670	0.246
PAC2 DR28-2	113.3	-47.51	2488	1656	-56.2	1397	8.6	191.77	0.57468	2.103
PAC2 DR29-1	113.1	-47.01	2407	2933	-68.2	439	17.1	171.94	0.68383	0.278
PAC2 DR30-1	112.9	-46.40	2345	2446	-60.1	385	14.9	164.14	0.66544	0.273
PAC2 DR31-3	112.7	-45.85	2414	1983	-65.5	530	12.7	156.74	0.61245	0.672
PAC2 DR32-1	112.4	-45.39	2384	2695	-61.0	356	16.2	166.78	0.69091	0.268
PAC2 DR33-1	112.3	-44.87	2374	2657	-56.8	294	16.2	164.05	0.70567	0.236
PAC2 DR34-1	112.0	-44.24	2467	1276	-61.4	1516	8.1	158.20	0.46939	3.042
PAC2 DR35-1a	111.8	-43.59	2463	4808	-51.7	259	24.9	192.85		0.183
PAC2 DR36-1	111.6	-42.95	2503	2804	-55.6	548	16.2	173.59	0.64663	0.440
PAC2 DR37-2	111.3	-42.27	2474	2462	-58.2	439	15.1	163.35		
PAC2 DR38-1	113.3	-41.8	2524	1751	-57.8	151	10.2	172.343		0.214

7. FIGURES CAPTIONS

Figure 1. Map of the sampling area, illustrating the position of the samples with respect to the local geographical and geological features. The symbols representing the samples will remain the same in the whole article. The figure was created with the GeoMapApp application and the depths databases included therein.

Figure 2. δD (in ‰, top panel) and water content (in ppm, bottom panel) along the sampling area. Error bars are smaller than the symbols for water content.

Figure 3. From top to bottom : H_2O/Ce, $^{206}Pb/^{204}Pb$, Cl content and Cl/K along the sampling area. Except south of Saint-Exupery fracture zone, all H_2O/Ce ratio are in the range of North Pacific basalts.

Figure 4. Water content as a function of eruption pressure and curves illustrating the composition of the vapor in equilibrium with the magma for a given water content and pressure. This figure illustrate that all but sample PAC1DR10-1 were not significantly affected by degassing.

Figure 5. Incompatible species content as a function of MgO wt%. From top to bottom, Ce, La, H_2O and Cl. Continuous lines are best linear fits, while dotted lines illustrate the differentiation trend predicted for a perfectly incompatible species. Note that we observe over-enrichement for H_2O, La and Ce, as commonly observed in numerous sample suites (e.g. Sours-Page et al., 1999). However the over-enrichment happens for both H_2O and Ce, as illustrated here and by the constant H_2O/Ce ratios, and is thus not due to an increase in assimilation with increasing differentiation.

Figure 6. Cl/H_2O versus Ce/H_2O and curves resulting from the addition

of seawater, brines with various concentrations or a serpentine with 10 wt.% H_2O, 1000 ppm Cl and 10 ppm Ce to a typical MORB composition (2000 ppm H_2O, $H_2O/Ce = 200$, 1000 ppm K, $K/Cl = 12.5$ (Kendrick et al., 2012)). The figure illustrate that the observed variations are not compatible with the addition of diluted brines, seawater or hydrated mafic rock. Shaded outlines illustrate the dispersion of the data in the southern (continuous outline) and the northern (dotted outline) supersegments.

Figure 7. Sodium content as a function of water content, both corrected to 8 wt.% MgO. Continuous lines represent constant water content in the source, and dotted lines correspond to constant melting rate. Both where calculated using a simple batch melting model with 0.29 wt.% of Na in the source (Klein and Langmuir, 1987; Kelley et al., 2006). We assumed incompatibilities of 0.012 for water (Aubaud et al., 2004; Kohn, 2006; Grant et al., 2007) and 0.02 for sodium (Kelley et al., 2006).

Figure 8. Ratios of water to Ce (top) and La (bottom) as function of Ce and La contents respectively. Straight lines are best linear fits and dotted lines represent the 95% confidence envelope.

Figure 9. From top to bottom, δD as a function of La/Sm_N, $^{206}Pb/^{204}Pb$ and TiO_2/H_2O. There are no correlation in the top two panels, while the negative correlation in the bottom panel is controlled by the two samples PAC1CV04 and PAC1CV07 (which may reflect source re-melting, see text).

8. FIGURES

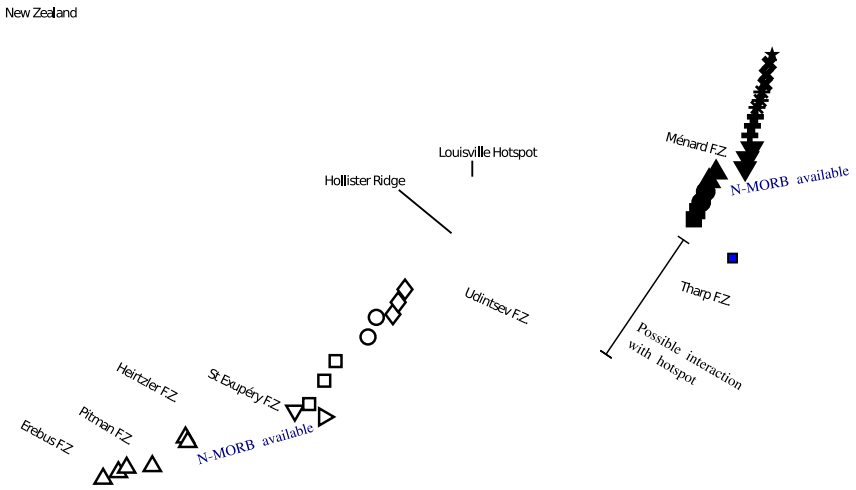

Figure 1:

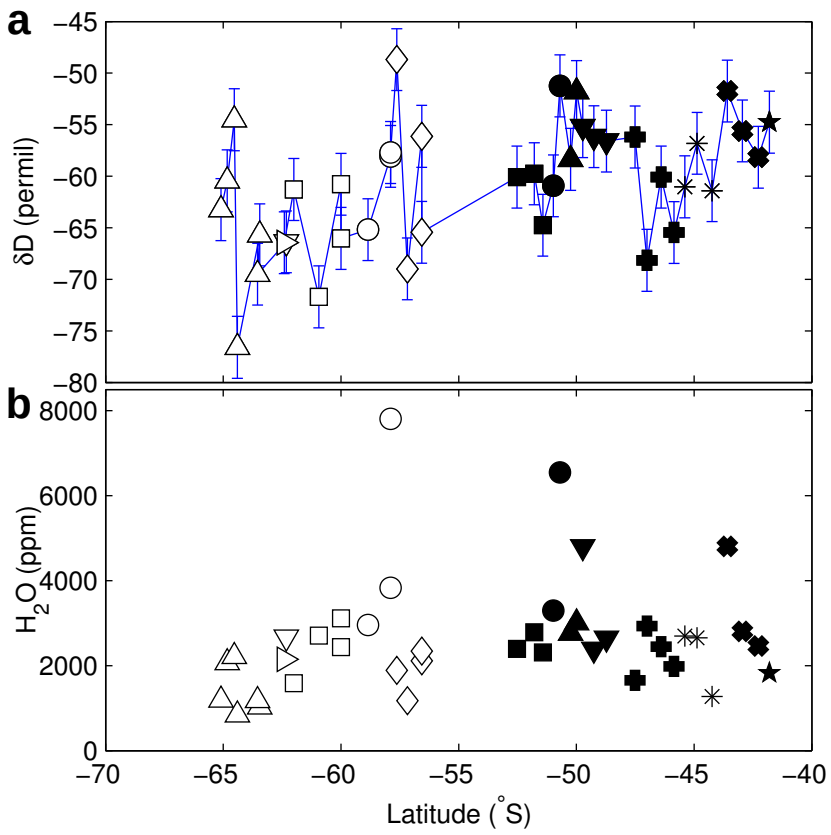
a
b
δD (permil)
H2O (ppm)
Latitude (°S)
−45
−50
−55
−60
−65
−70
−75
−80
8000
6000
4000
2000
0
−70
−65
−60
−55
−50
−45
−40

Figure 2:

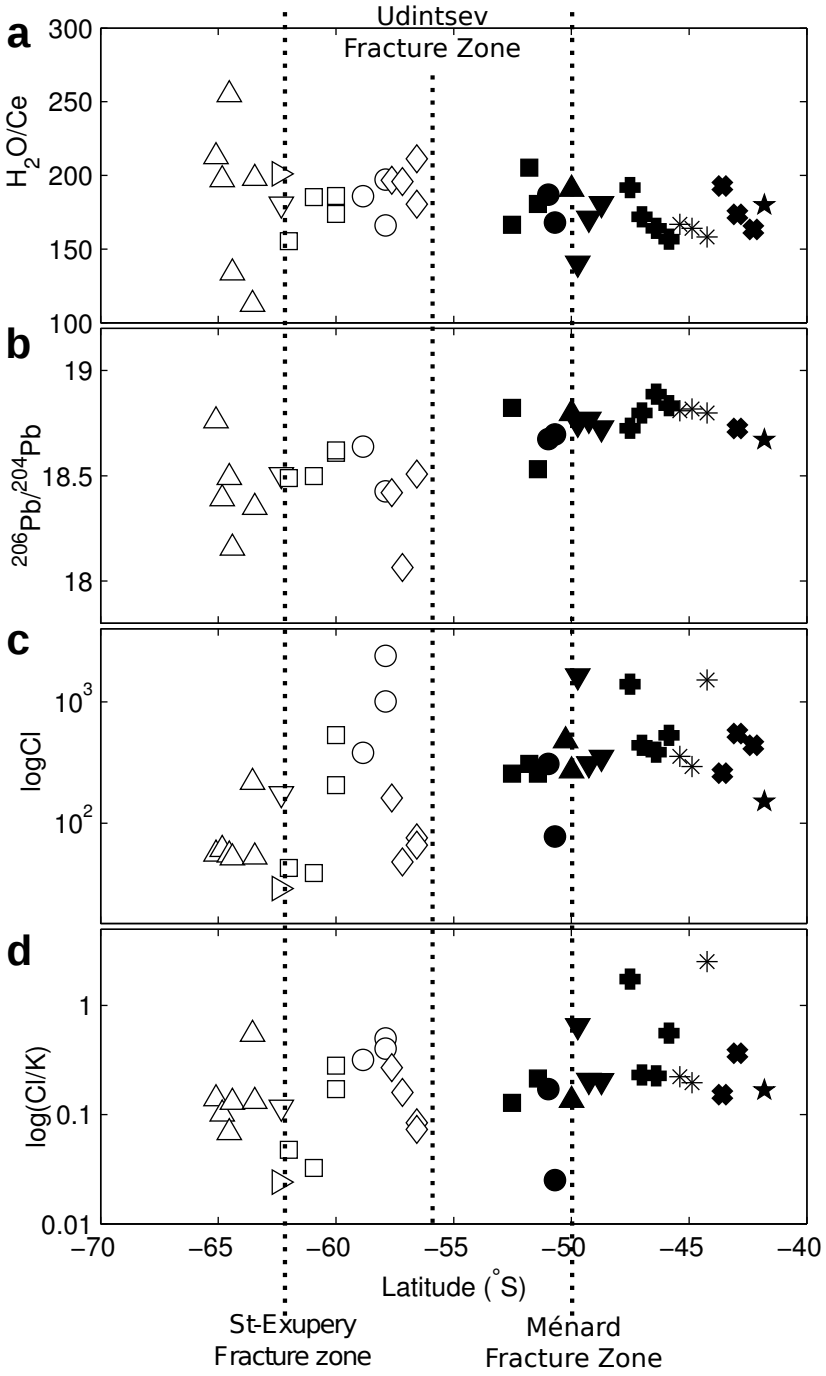
a
b
c
d
Udintsev
Fracture Zone
H_2O/Ce
$^{206}Pb/^{204}Pb$
logCl
log(Cl/K)
300
250
200
150
100
19
18.5
18
10^3
10^2
1
0.1
0.01
−70
−65
−60
−55
−50
−45
−40
Latitude (°S)
St-Exupery
Fracture zone
Ménard
Fracture Zone

Figure 3:

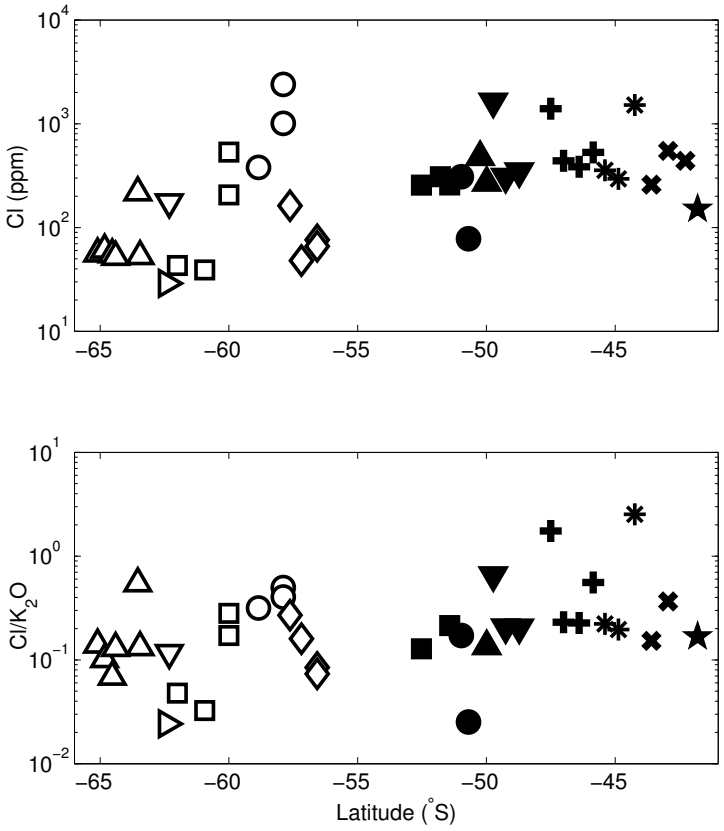
Cl (ppm)
10^4
10^3
10^2
10^1
−65
−60
−55
−50
−45
Cl/K_2O
10^1
10^0
10^{-1}
10^{-2}
−65
−60
−55
−50
−45
Latitude (°S)

Figure 4:

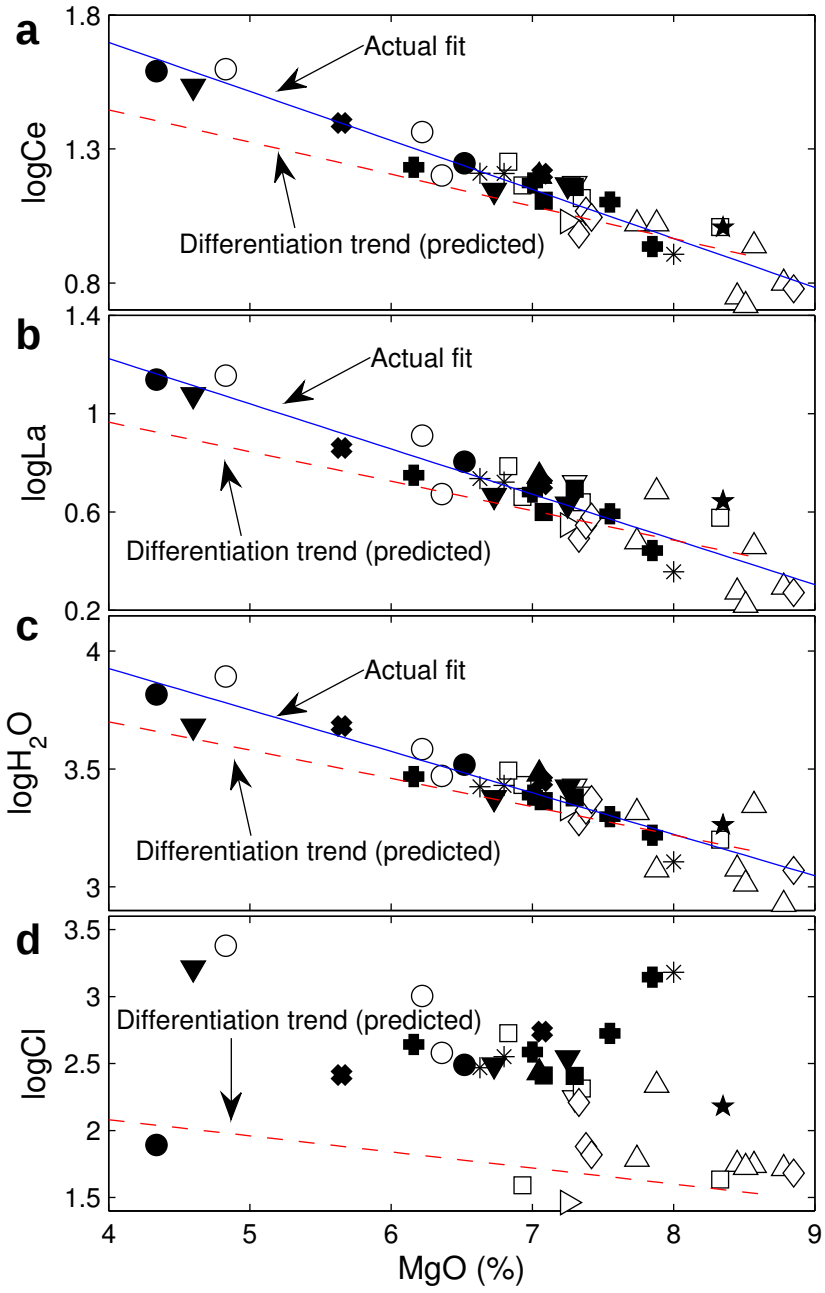
a
b
c
d
logCe
logLa
logH2O
logCl
Actual fit
Differentiation trend (predicted)
MgO (%)
1.8
1.3
0.8
1.4
1
0.6
0.2
4
3.5
3
2.5
2
1.5
5
6
7
8
9

Figure 5:

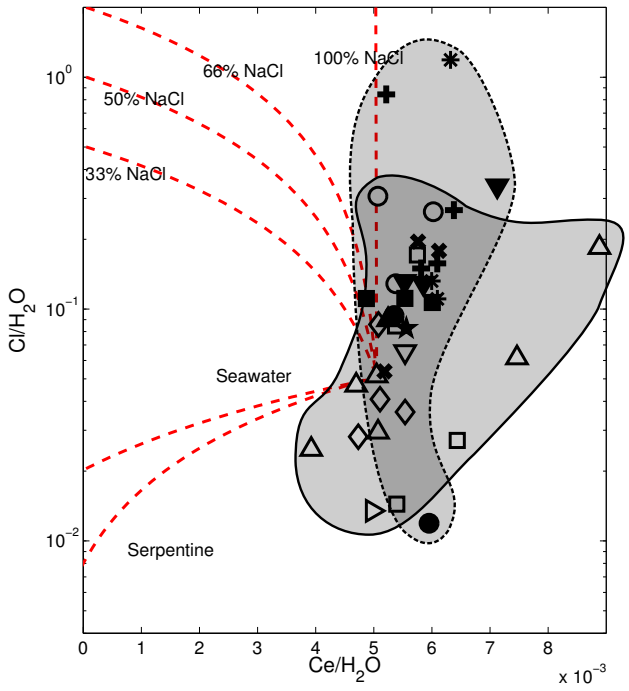
100% NaCl
66% NaCl
50% NaCl
33% NaCl
Seawater
Serpentine
Cl/H2O
Ce/H2O
x 10−3
10^0
10^−1
10^−2
0
1
2
3
4
5
6
7
8

Figure 6:

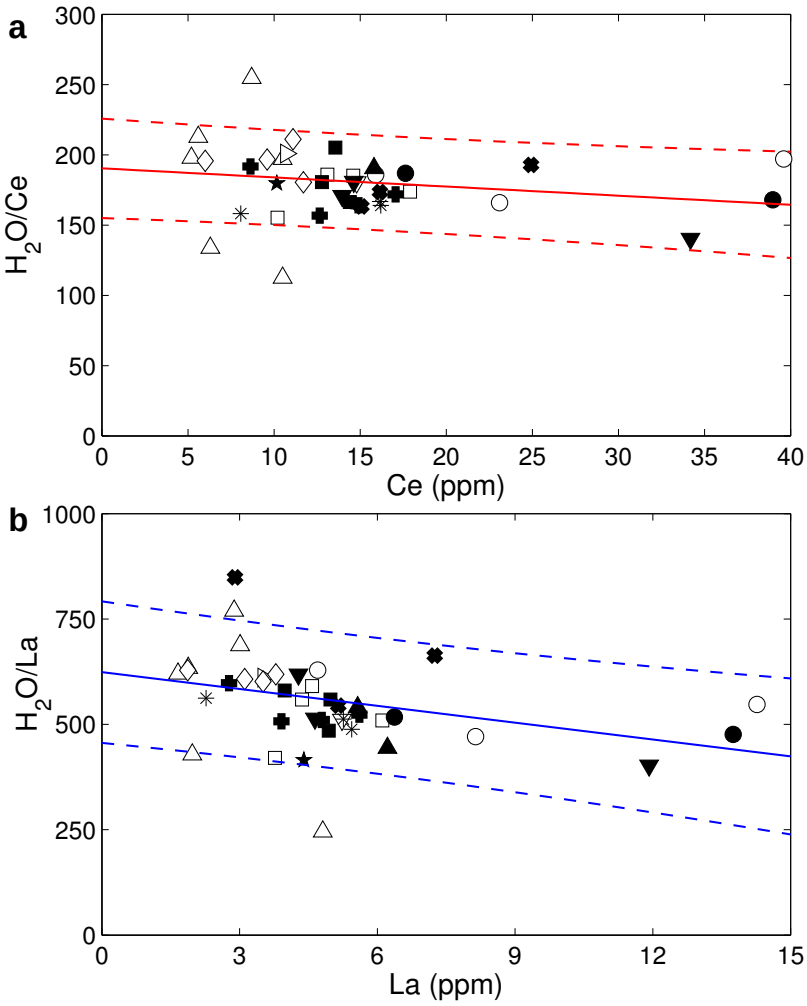
a
300
250
200
150
100
50
0
H2O/Ce
0
5
10
15
20
25
30
35
40
Ce (ppm)
b
1000
750
500
250
0
H2O/La
0
3
6
9
12
15
La (ppm)

Figure 7:

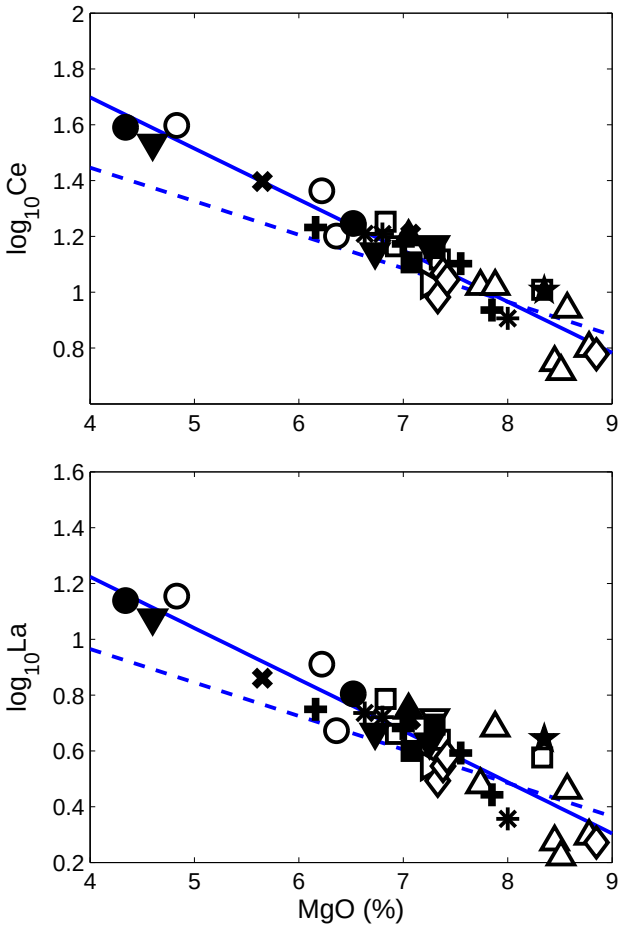

Figure 8:

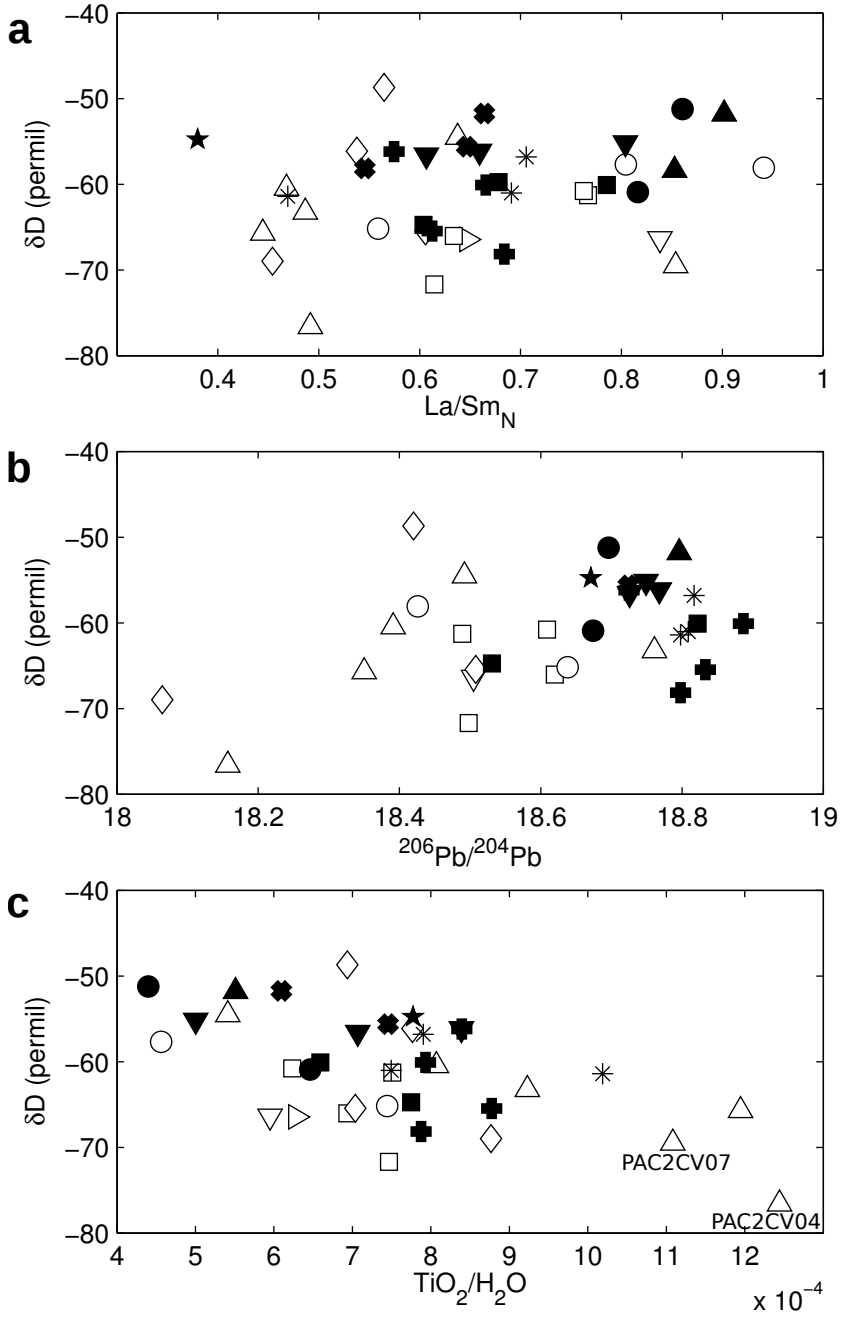
a
δD (permil)
−40
−50
−60
−70
−80
0.4
0.5
0.6
0.7
0.8
0.9
1
La/Sm$_N$
b
δD (permil)
−40
−50
−60
−70
−80
18
18.2
18.4
18.6
18.8
19
^{206}Pb/^{204}Pb
c
δD (permil)
−40
−50
−60
−70
−80
PAC2CV07
PAC2CV04
4
5
6
7
8
9
10
11
12
TiO$_2$/H$_2$O
x 10^{-4}

Figure 9: